Tens-of-PeV photon search at the Pierre Auger Observatory with the Underground Muon Detector

Nicolás González
Instituto de Tecnologías en Detección y Astropartículas

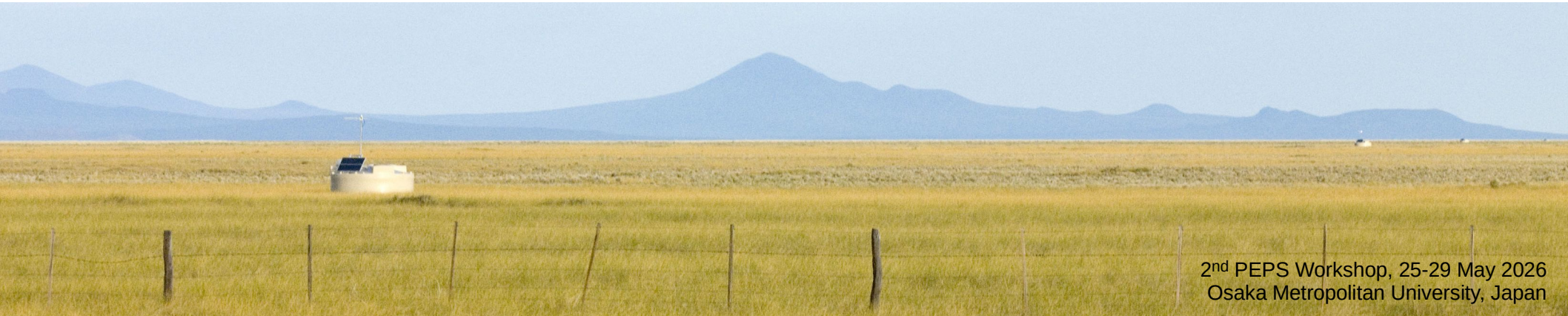

2nd PEPS Workshop, 25-29 May 2026
Osaka Metropolitan University, Japan

Photon search at tens of PeV

► 10-PeV diffuse photons from:
- hadronic interactions in hot gas at the Galactic halo
- super-heavy dark matter decay at the Galactic center
- propagation of UHE cosmic rays

► Highest-energy photons measured by LHAASO at ~ 1 PeV. Upper limits on the diffuse photon flux between 1-150 PeV were set only from the Northern Hemisphere

► **The result**: the most stringent upper limits to the photon flux above 50 PeV to 150 PeV having a privileged exposure to the Galactic center

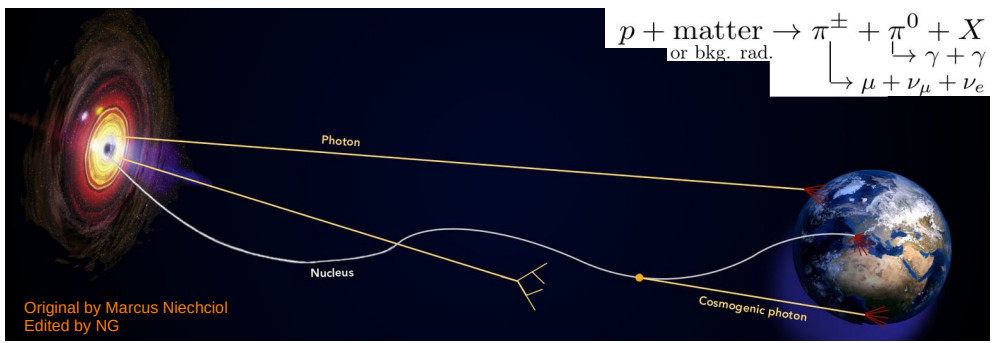

JCAP 05 (2025) 061

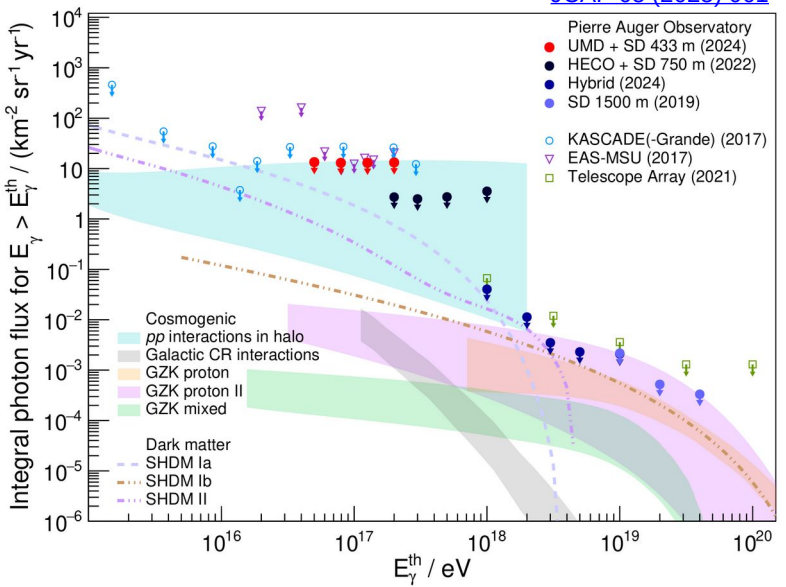

How did we do it?

► 433-m surface detector (shower detection)

► Undeground muon detector (discrimination)

SD-433 is sensitive to cosmic rays at tens of PeV

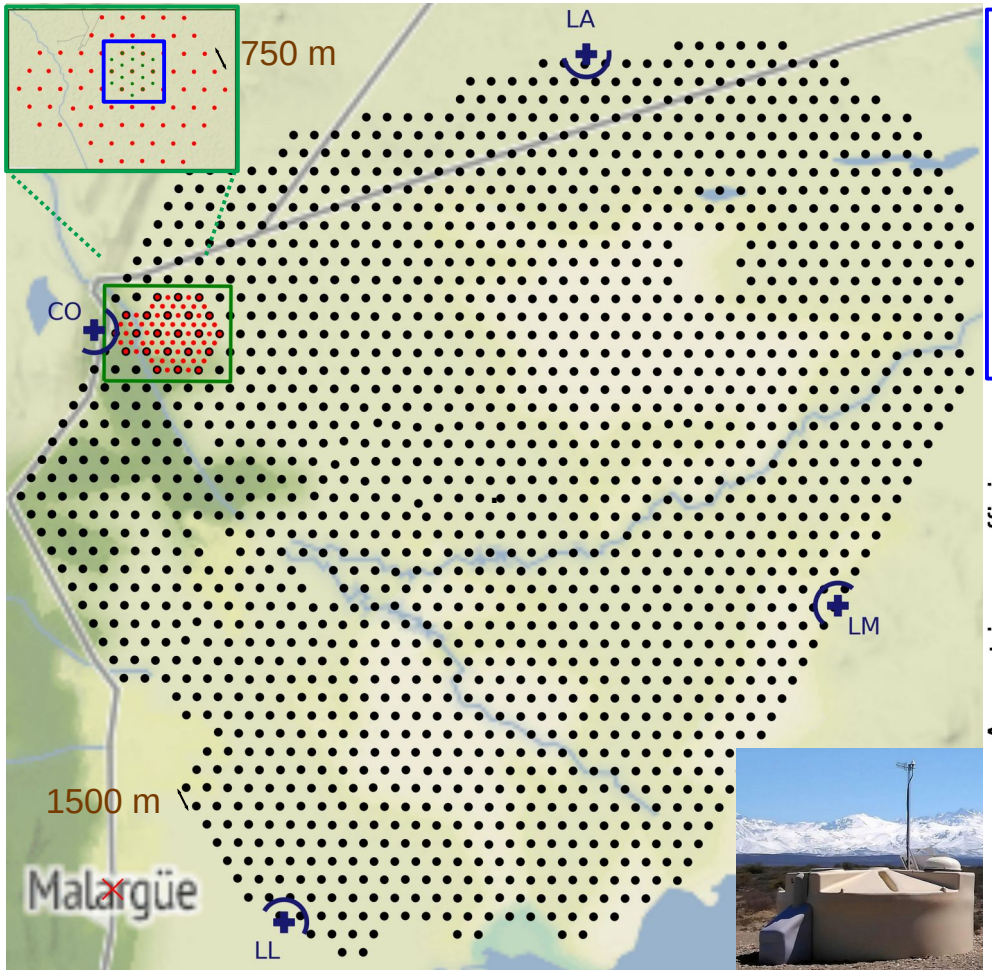

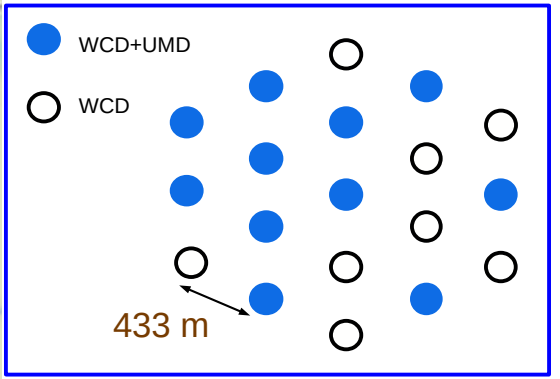

► Systematically smaller trigger efficiency in photon events due to the scarcer muon component

► 88% (92%) of trigger efficiency for photon (proton) events above 50 PeV and θ < 52°

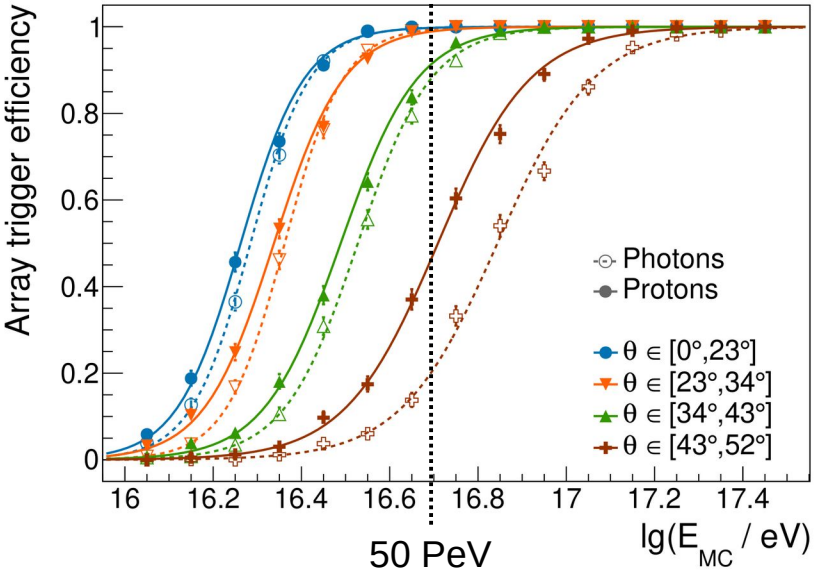

Photon-equivalent energy scale

► A unified energy scale is essential for accurately comparing events initiated by different primary species

► **Solution of compromise**: a “mid-point” method combining both dedicated energy calibrations

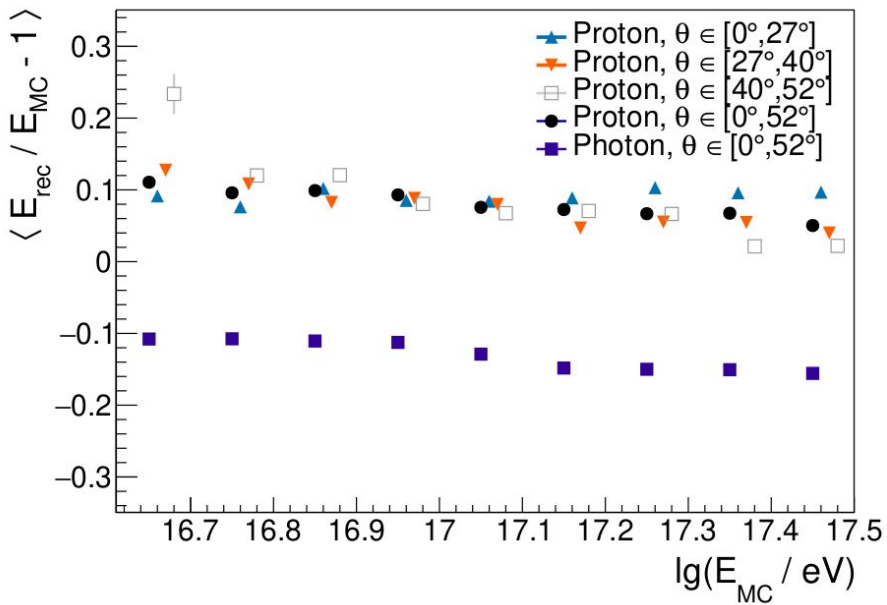

$$\frac{S(250)}{g'(\theta)} = \left(\frac{E_{\mathrm{MC}}}{10^{17}\,\mathrm{eV}}\right)^{\alpha(\theta)}$$

Photon

Proton

► If reconstructed with the photon scale, proton events have a 15% bias (due to muonic component in hadronic showers)

► Minimal angular dependence for bkg events at the expense of a mild bias for both classes of events

► In a given $E_{\gamma,eq}$ bin, protons with lower true energy coexist with photons with higher true energy

→ a conservative scenario for discrimination

The Underground Muon Detector

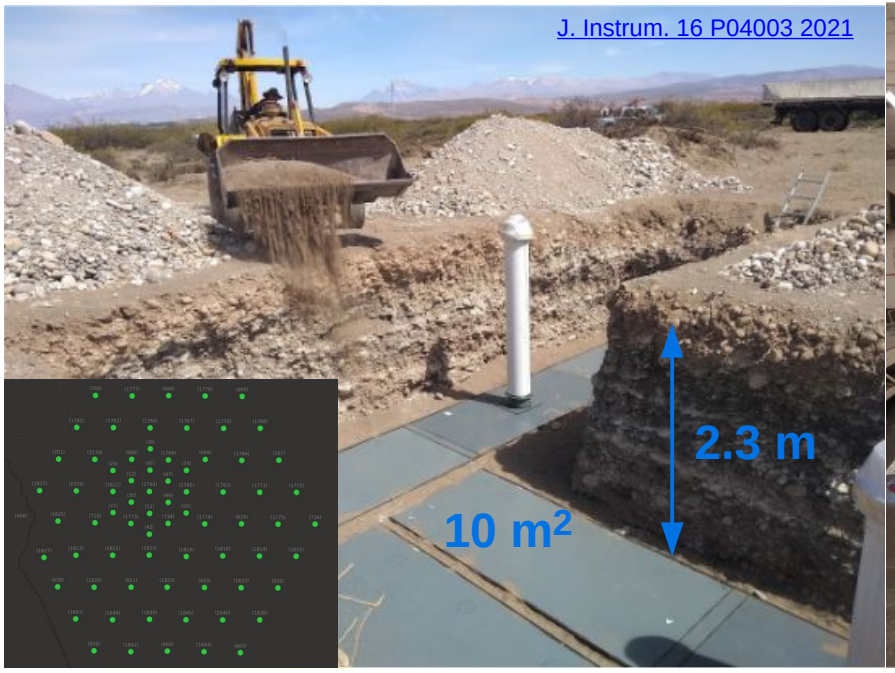

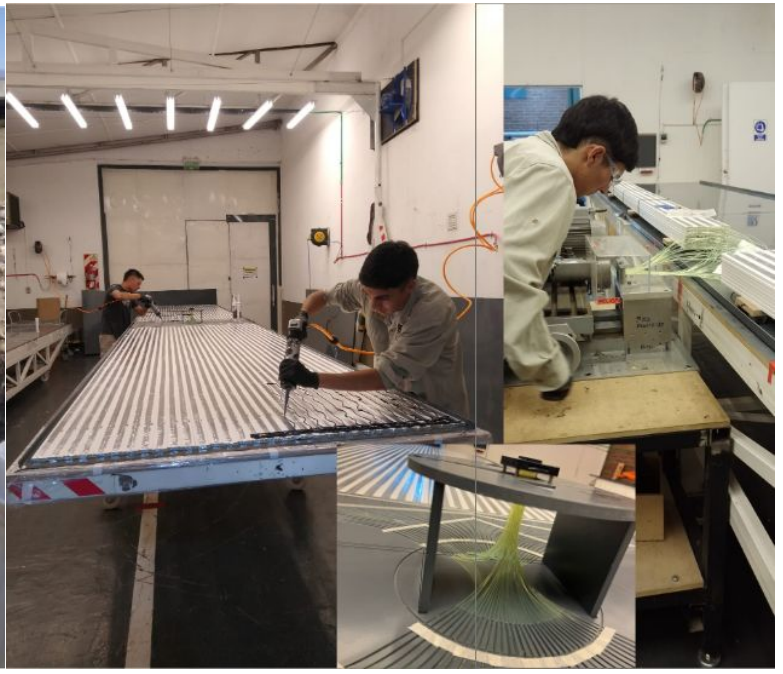

► 1 station = 3 x 10 m^2 modules = 64 plastic scintillation bars

► All charged particles from the air-shower are filtered in the ground, except muons

► Direct counting of air-shower muons by measuring fluorescence light yield produced by traversing particles

► Single-pixel silicon photomultipliers (SiPM) as optosensors

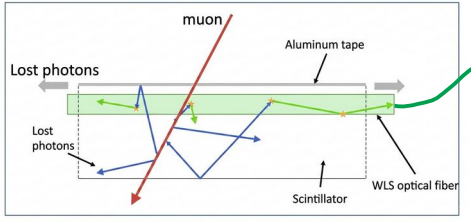

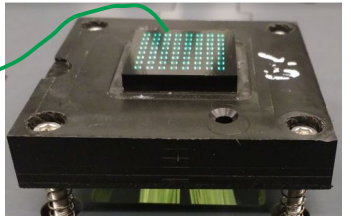

Overview of UMD electronics

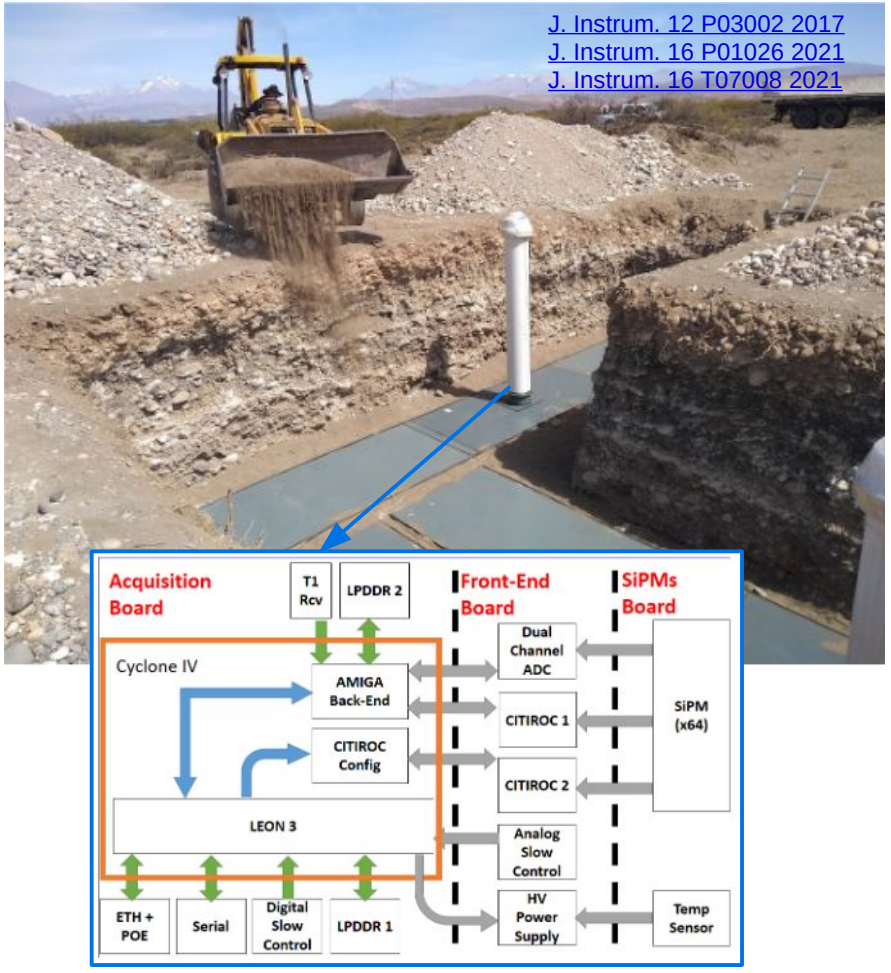

SiPMs board

► Receiver of the 64 SiPMs signals

► Includes an on-board temperature sensor to enable real-time high voltage (HV) compensation in the power supply, ensuring stable gain despite temperature fluctuations.

Front-End board

► CITIROC ASICs: manages 64 optical channels with an integrated fast shapers designed to match SiPM pulse widths and prevent muon pile-up

► Integrated slow control to monitor all on-board supply voltages in real-time

Acquisition board

►FPGA-based embedded system hosting a microprocessor. Hosts firmware, Linux-based boot image, and acquisition software

►Handles the trigger and clock signals received from the SD station

The two independent modes of the UMD

Counter mode

► One-bit electronics: scintillation light converted to digital traces by comparing to a pre-selected voltage threshold
► Muon counting strategy to estimate the number of muons
► Optimized for low muon densities (O(1)μ / 10 m^2)

J. Instrum. 16 P07059 2021

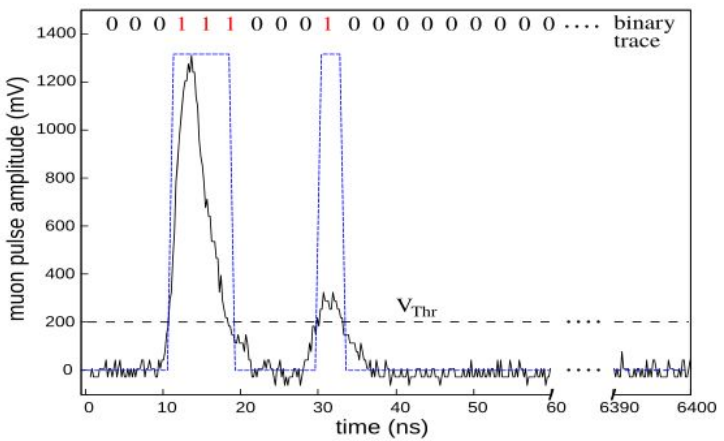

Fig. 3 The counting procedure: a muon pulse (black) is discriminated, and the discriminator signal (dashed blue) is then digitally sampled by an FPGA every 3.125 ns up to 6.4 μs. As a result, the binary trace on the top of the figure is obtained

Integrator mode

► Sensitive to the amount of collected light
► Total measured signal converted to number of muons through calibration histograms
► Optimized for high muon densities (>64 μ / 10 m^2)

EPJ Web of Conf. 283, 06012 2023

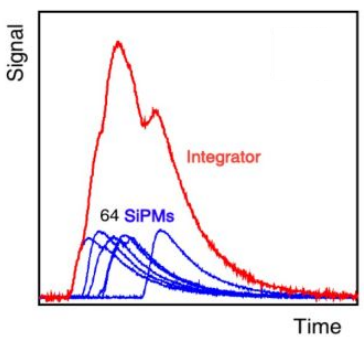

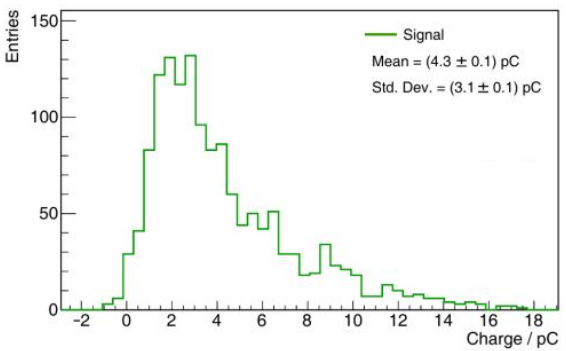

Long-term monitoring

Proc. Sci., 501, 176, ICRC25

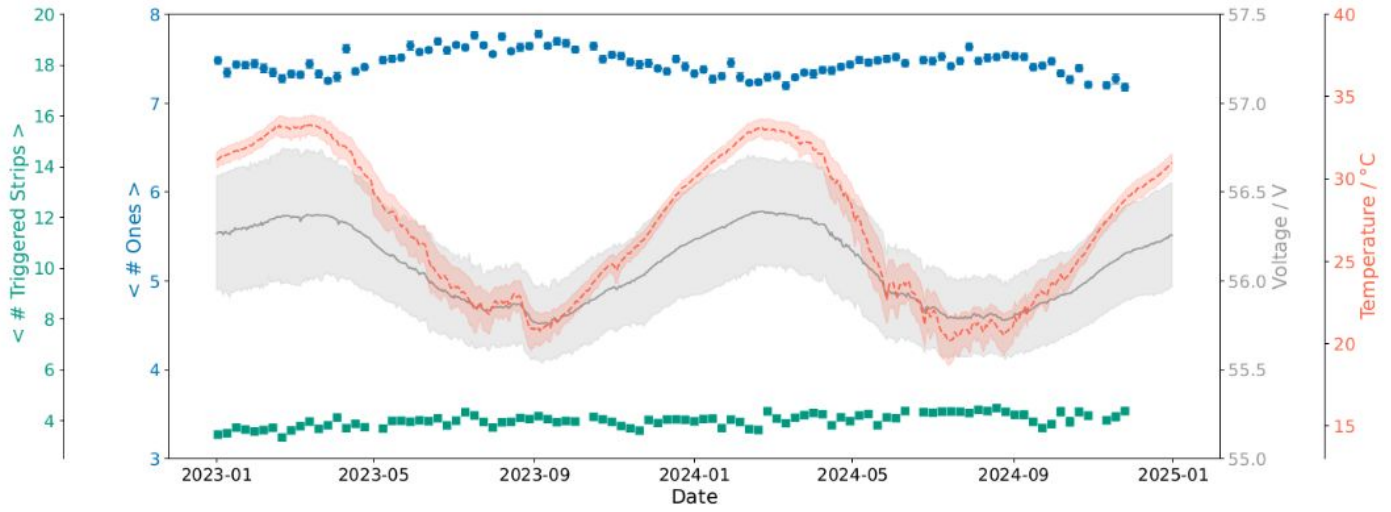

► A seasonal trend is observed in both temperature and voltage, as expected from the environmental modulation at the site

► Automatic high-voltage compensation applied to SiPM breakdown voltage ensures that the average number of triggered strips per event remains stable over time

► The muon pattern recognition and event-level response are not compromised by environmental fluctuations

Recent developments in UMD data analysis

From digital traces to muon density measurements: systematic effects studied and corrections were designed

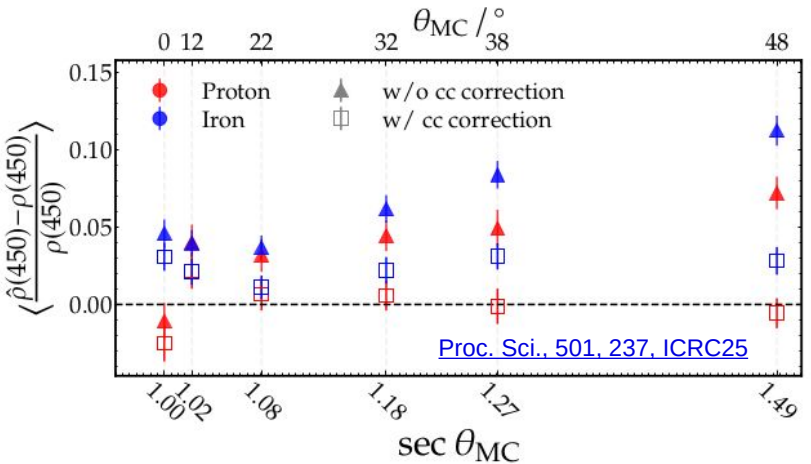

Refined binary mode precision: Data-driven corrections for corner-clipping muons and leaving the shower core position free during event reconstruction, have kept **muon shower size, ρ(450), bias below 3%**

Proc. Sci., 501, 389, ICRC25

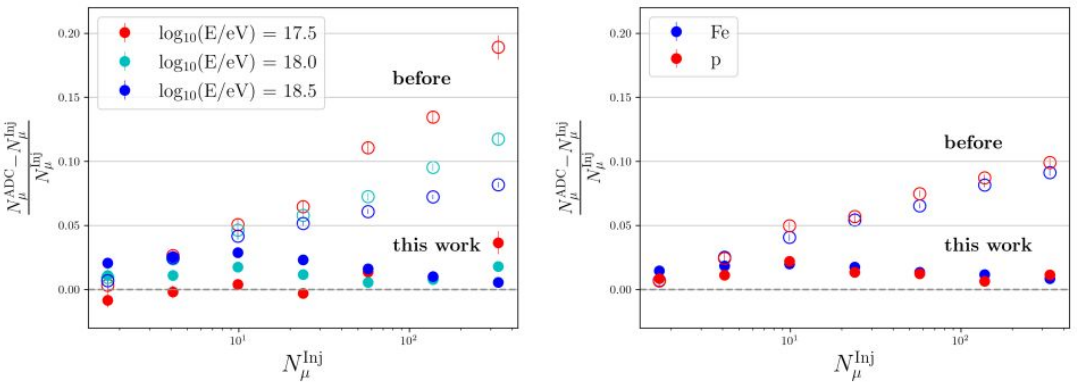

Significant bias reduction in integrator mode: Accounting for energy deposition from knock-on electrons generated in the soil, **reconstruction bias** has been reduced from 20% **to less than 5% across all energies**, primary masses, and zenith angle

M_1: the discrimination observable

► Discrimination based on the muon density, ρ_i, measured by the UMD stations (in counter mode)

► M_1 calculated with the UMD stations of the hottest hexagon

► The normalization factor ρ_{pr} is the expected muon density for proton events at r_{pr} = 200 m

$$M_1 = \lg\left(\sum_i \frac{\rho_i}{\rho_{\mathrm{pr}}} \times \left(\frac{r_i}{r_{\mathrm{pr}}}\right)\right)$$

Astropart. Phys. 114, 48-59, 2020

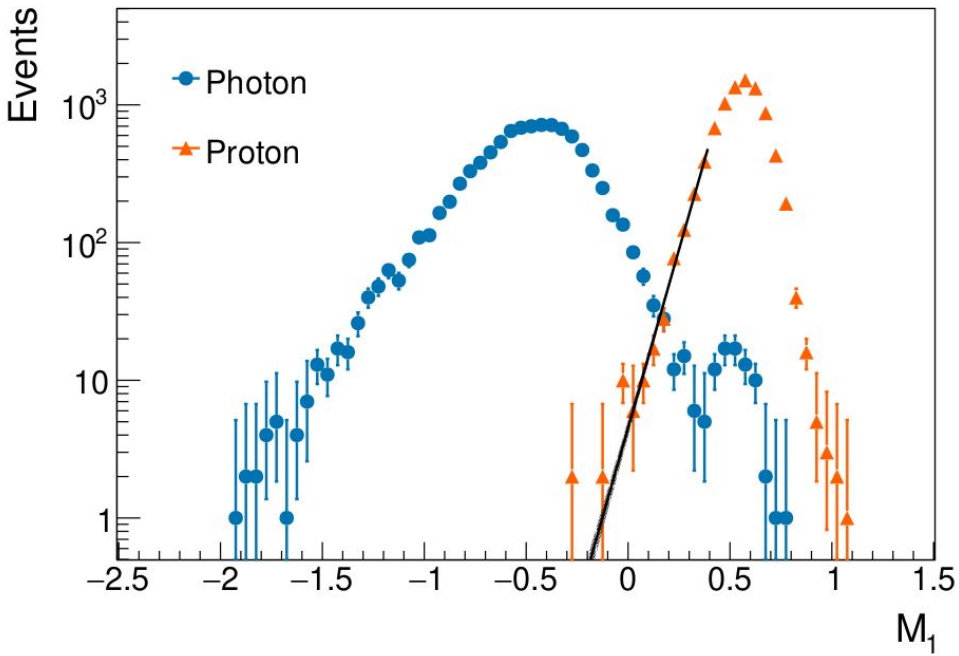

M_1 performance

- Two metrics characterize the discrimination performance:

$$\text{bkg. contamination} = \int_{-\infty}^{x} f_{\text{pr}}(M_1) dM_1$$

$$\text{sig. efficiency} = \int_{-\infty}^{x} f_{\gamma}(M_1) dM_1$$

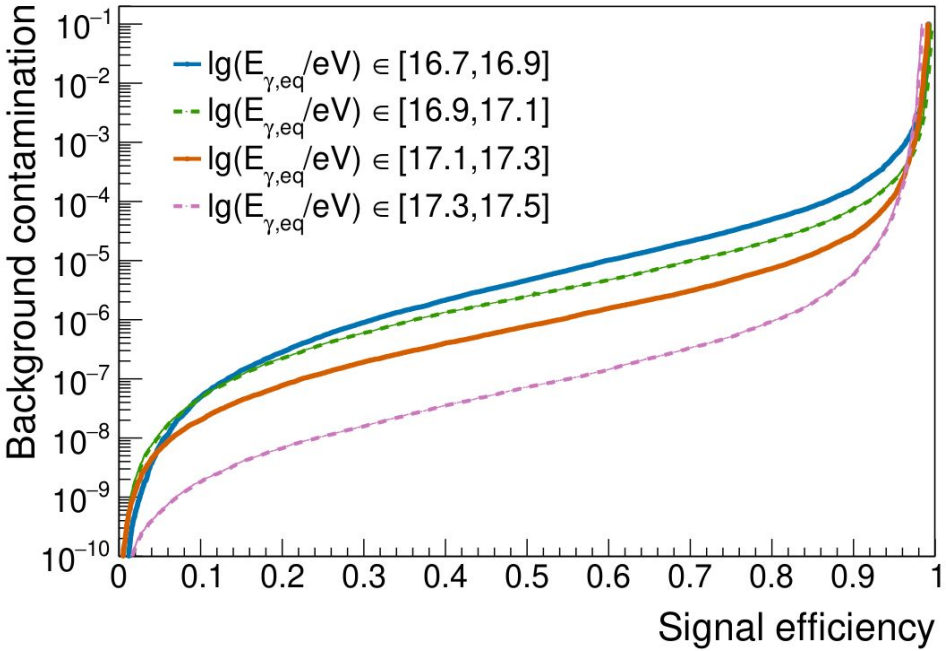

- Contamination decreases with increasing primary energy due to the larger air-shower muon content

- Larger signal efficiency at the expense of larger contamination

Data classification

SD-433+UMD (2020-2022)

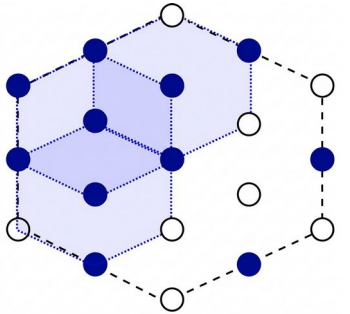

► Since M_1 scales with the number of muon density measurements, any missing UMD station would bias M_1

→ event classification in six “categories” based on number and placement of available UMD stations

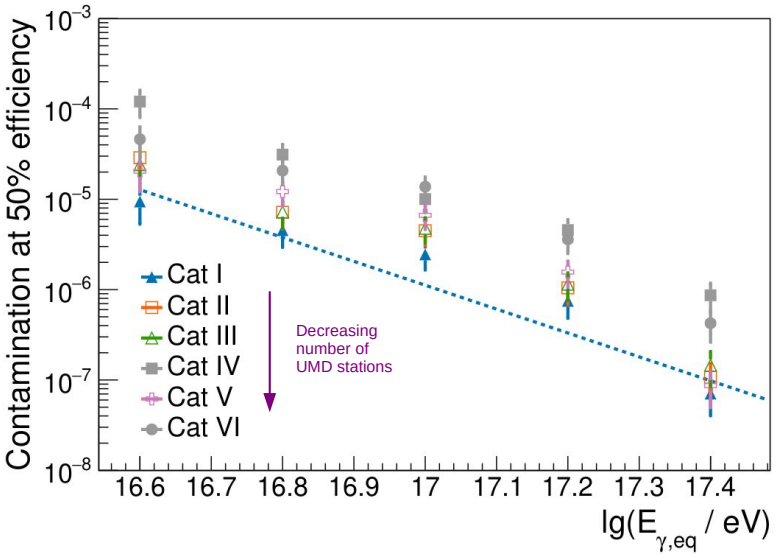

► Contamination increases for decreasing number of UMD stations

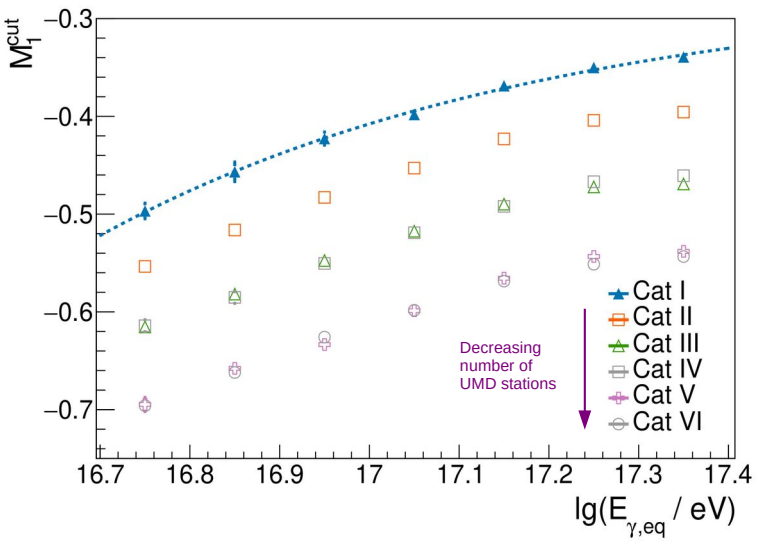

► M_1^{cut} is the threshold value at which a 50% signal efficiency is reached

Full data-set unblinding: no photon candidates

► Events for each of the six categories. Lines correspond to the parametrized M_1^{cut} (the “photon candidate cuts”)

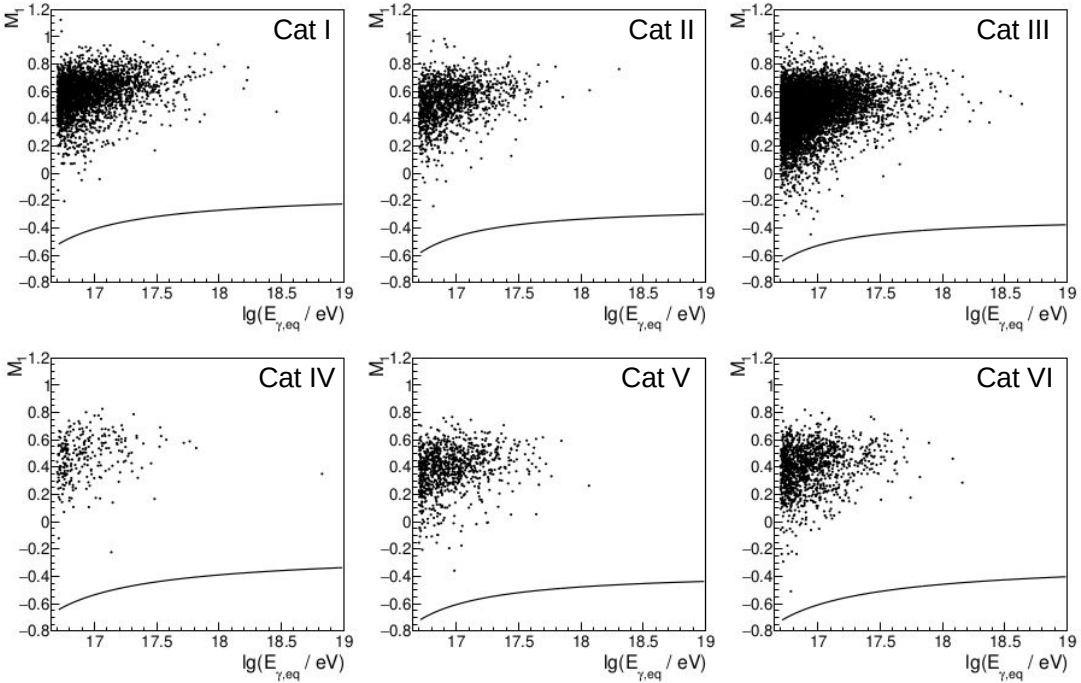

► No events below the photon candidate cuts
→ upper limits to the photon flux, Φ_γ, above E_γ^{th}

$$\Phi_\gamma < \frac{3.095}{(1 - f_{\mathrm{burnt}}) \times f_{\mathrm{cut},\gamma} \times \epsilon_\gamma}$$

► f_{burnt} = 0.1 (fraction of burnt data)
► $f_{cut,\gamma}$ = 0.504 (signal efficiency)
► ε_γ, exposure to photons

E_γ^{th} (PeV)	ϵ_γ (km^2 sr yr)	Φ_γ (km^{-2} sr^{-1} yr^{-1})	$\Phi_\gamma + \sigma_{\mathrm{sys}}$ (km^{-2} sr^{-1} yr^{-1})
50	(0.58 ± 0.02)	12.3	13.8
80	(0.61 ± 0.03)	11.7	13.5
120	(0.63 ± 0.03)	11.3	13.3
200	(0.63 ± 0.03)	11.3	13.6

► Upper limits increased by:
- energy bias of the photon-equivalent scale (12-17)%
- variations in the spectral index (0.8-2.2)%
► No impact from muon deficit or UMD simulation

The AugerPrime Upgrade

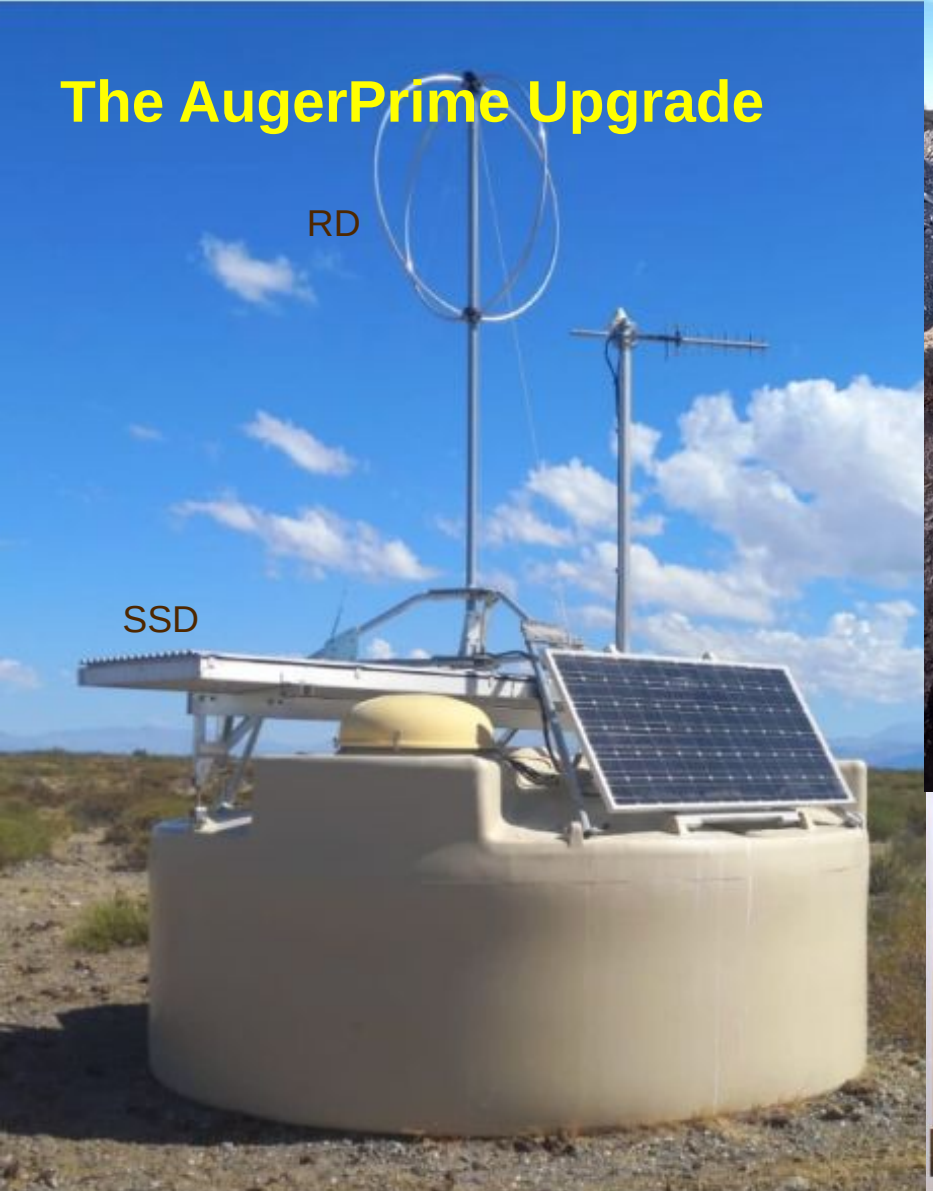

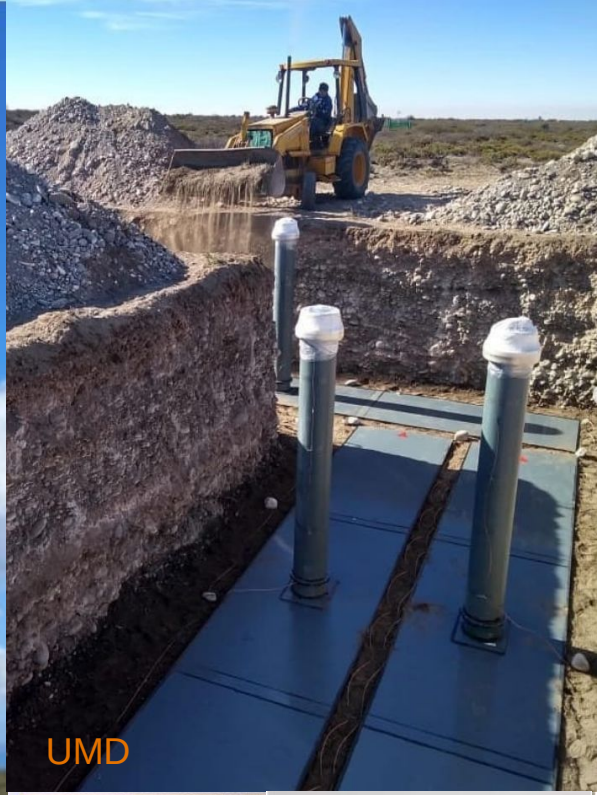

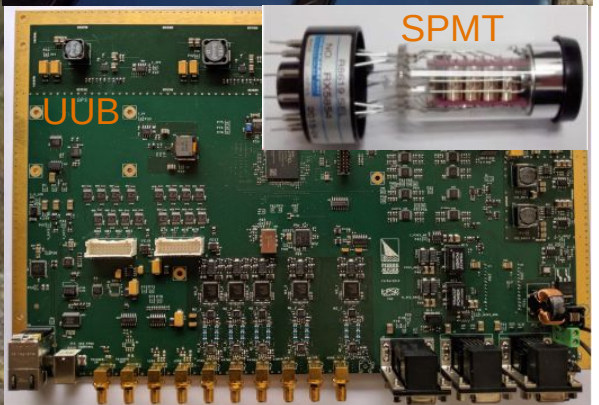

► The results shown before were obtained with only ~1.5 years of data.

► The AugerPrime upgrade improves the composition sensitivity (including UHE γ)

Multi-hybrid air-shower detection:

► 433 and 750 m SD arrays equipped with 3 x 10 m^2 UMD stations

► 4 m^2 plastic surface scintillation detectors (SSD)

► Measure radio emission from air showers with antennas (RD)

► Faster electronics (UUB) and larger dynamic range thanks to a small-area PMT (SPMT)

Proc. Sci., 501, 385, ICRC25

Possible synergies with PEPS

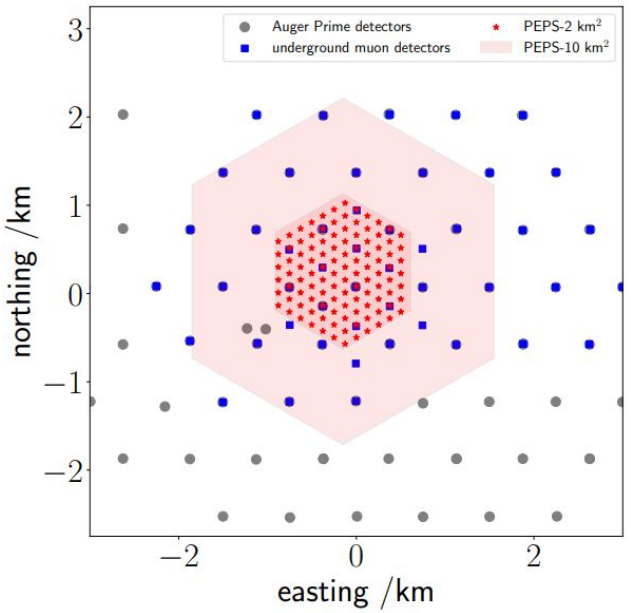

Proc. Sci., 501, 354, ICRC25

► **Muon-based separation & cosmic-ray composition sensitivity**:

dense low-energy-muon measurements (bottom layer of the WCDs)
+
sparse high-energy-muon measurements (UMD)

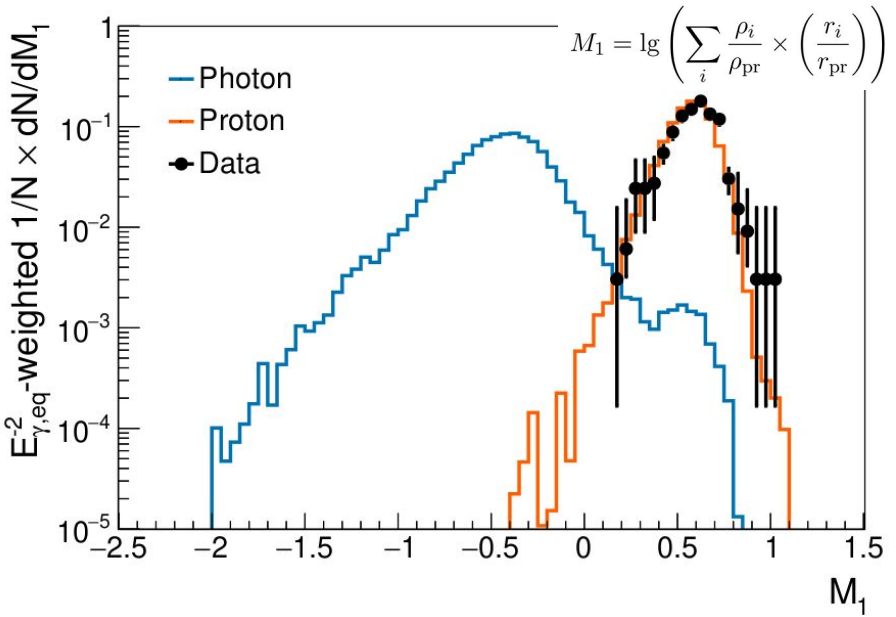

Possible synergies with PEPS

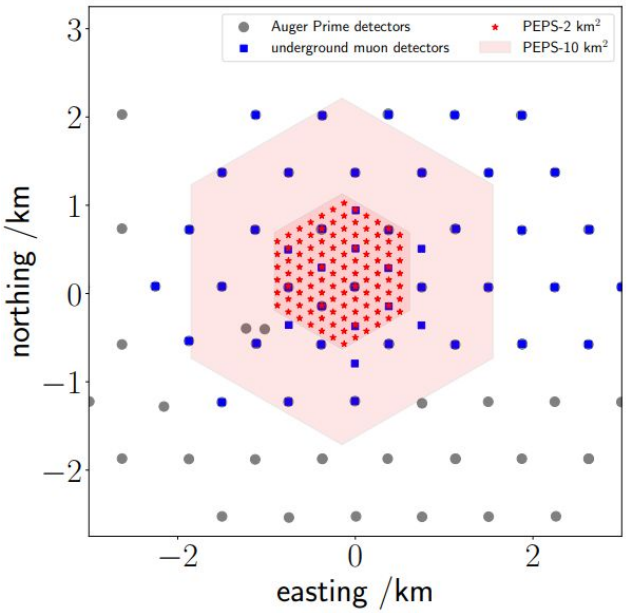

Proc. Sci., 501, 354, ICRC25

► **Architecture based on Graph Neural Networks (GNNs)**:

temporal structure of the WCD traces
+
high-energy muon density measurements

Proc. Sci., 501, 825, ICRC25

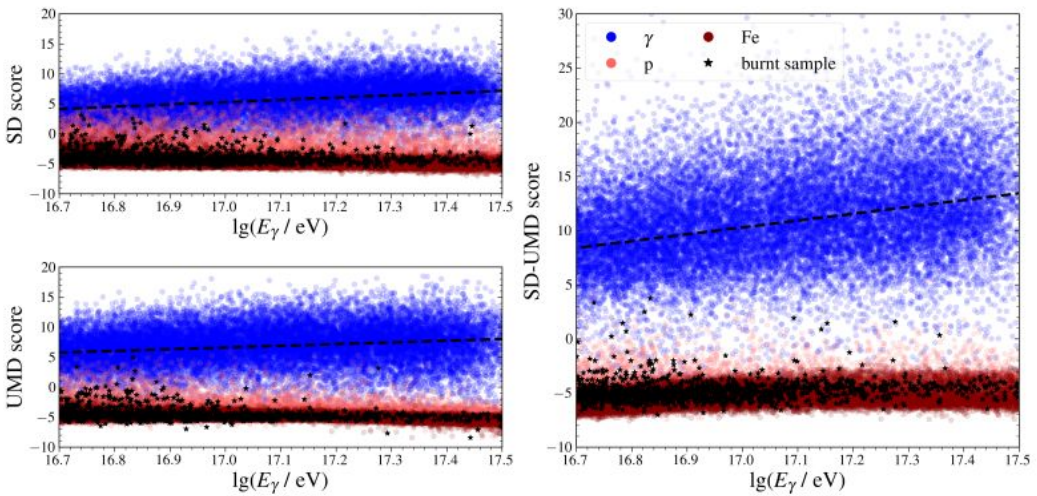

► Discrimination improved by using temporal features extracted with GNNs

► The layered WCD allows disentangling the EM and muonic components of the shower signal, enriching the discrimination power available to the GNN

Summary & outlook

► First search for a diffuse flux of primary photons above 50 to 200 PeV from the Southern Hemisphere

► Opportunity to constrain the mass-lifetime phase-space for specific super-heavy dark matter models and to explore the photon flux from proton-proton interactions in the Galactic halo

► Groundwork for a nearly real-time search for primary photons in the tens of PeV domain

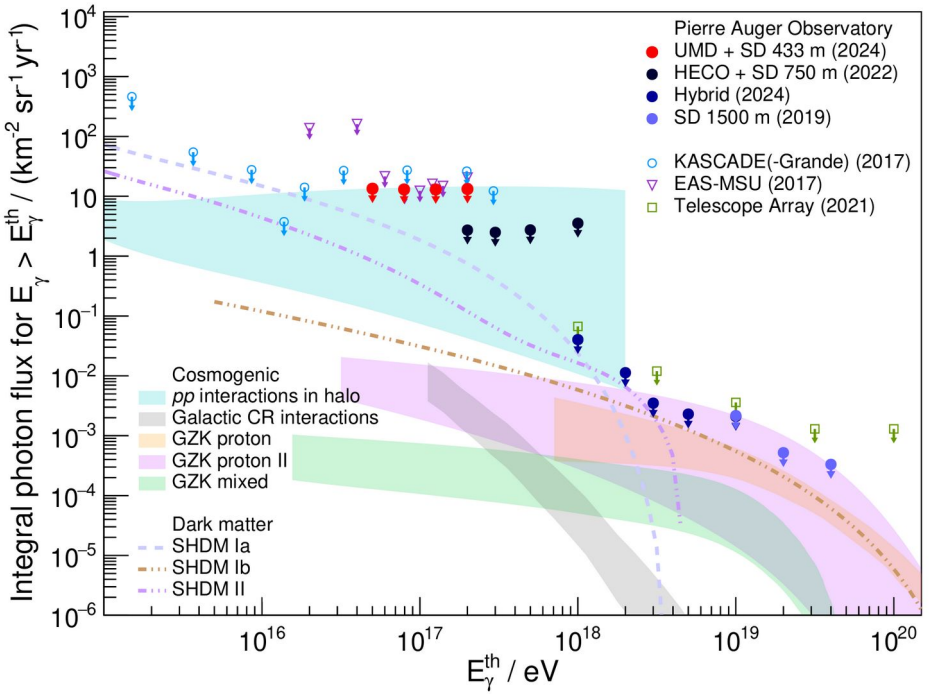

But what's next?

► Four more years of data available after this article

► AugerPrime photon search is under development. First results planned to be shown in the ICRC 2027

► The methodology discussed here (muon-based discrimination, GNN-based classification, photon-equivalent energy scale) provides a direct blueprint for a photon search with PEPS, at lower energies and higher statistics

Backup

Separation based on an estimate of the muon content

$$M_1 = \log_{10}\left(\sum_i \frac{\rho_\mu^i}{\rho_\mu^{\mathrm{p}}} \times \frac{r_i}{200\,\mathrm{m}}\right)$$

- M_1 combines the high-energy muon densities, ρ_μ^i, measured in the UMDs at a distance r_i from the shower axis.

- Separation based on the difference to a parametrization of the muon density at 200 m from the shower axis for proton, ρ_μ^p

- ρ_μ^p includes the effects of the atmospheric absorption of the muonic component.

- Positive values of M_1 expected for hadronic showers and negative values for photon showers

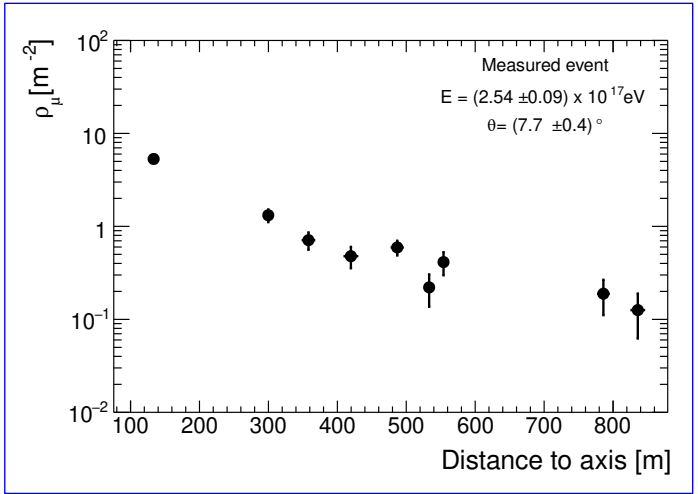

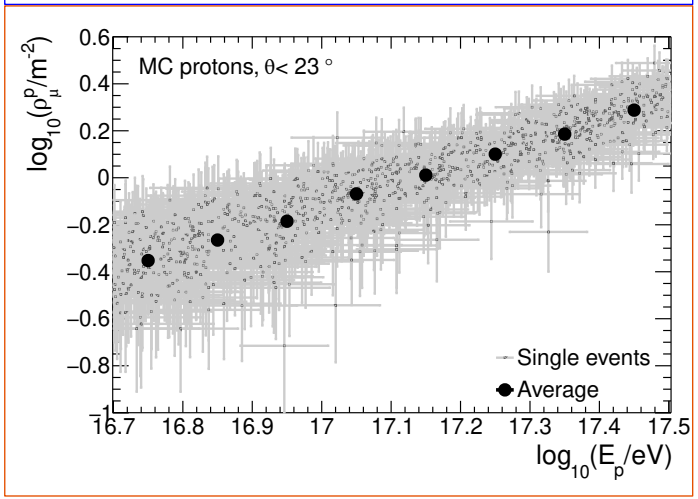

M_1 iron distributions

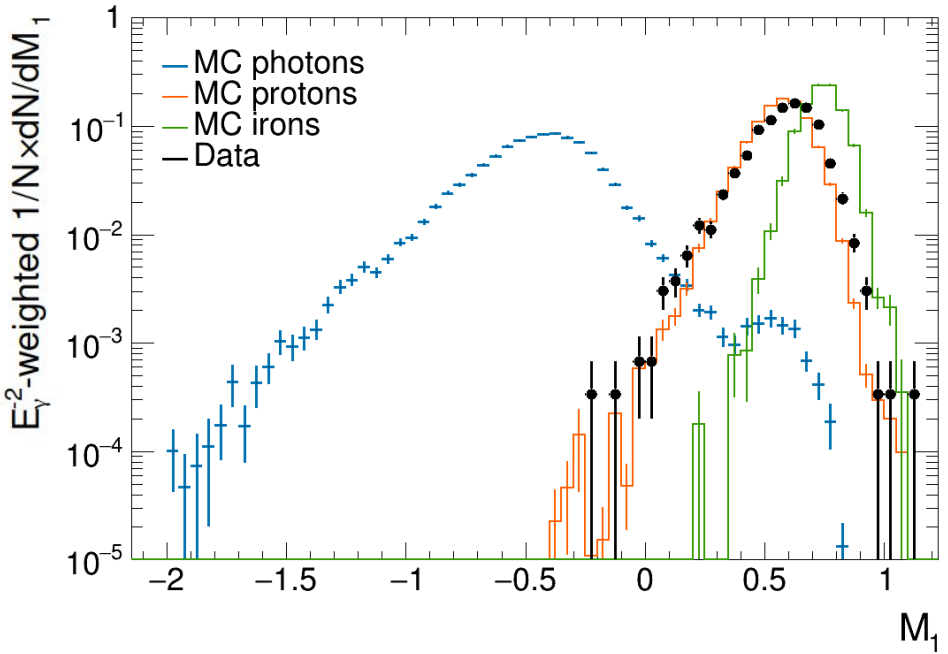

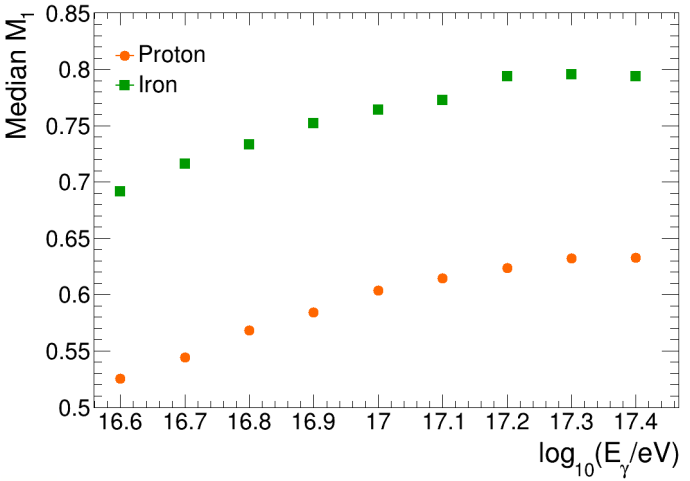

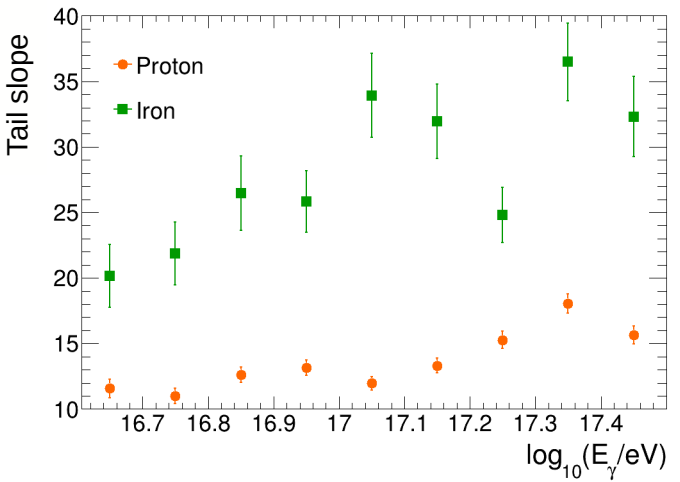

- Iron showers have more muons and fewer fluctuations
  → larger M_1 and steeper tail slopes
- Both features lead to smaller bkg contamination
- Note that iron MC set size is 25% of the protons one

Event categories

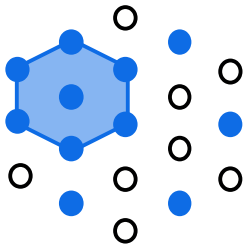

Cat I: 6 first-crown UMD stations

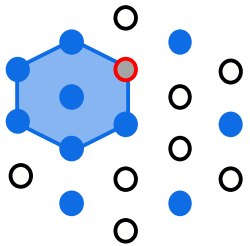

Cat II: 5 first-crown UMD stations

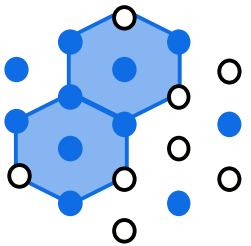

Cat III: 4 first-crown UMD stations, 2 isolated missing UMD stations

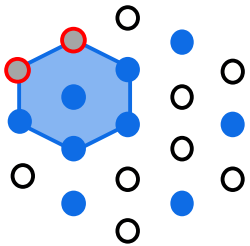

Cat IV: 4 first-crown UMD stations, 2 neighboring missing UMD stations

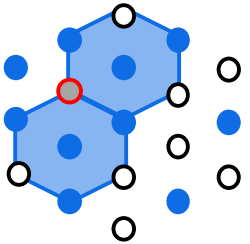

Cat V: 3 first-crown UMD stations, 3 isolated missing UMD stations

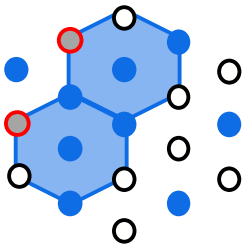

Cat VI: 3 first-crown UMD stations, 2 neighbouring missing UMD stations

Event categories

Cat.	No. of first-ring UMD stations	Minimum UMD area in first ring (m^2)	Missing UMD stations in first ring	No. of events
I	6	190	0	3,295
II	5	140	1	1,491
III	4	110	2 non-NN	8,417
IV	4	110	2 NN	298
V	3	80	3 non-NN	1,016
VI	3	80	2 NN + 1 non-NN	1,402
Total				15,919

Table 4. The six categories of events based on the available UMD stations in the hottest hexagon, the total detector area, and the relative location of missing UMD stations in the first ring, either nearest neighbors (NN) or non nearest neighbors (non-NN). The last column contains the size of each data subset.

Burnt sample is compatible with background

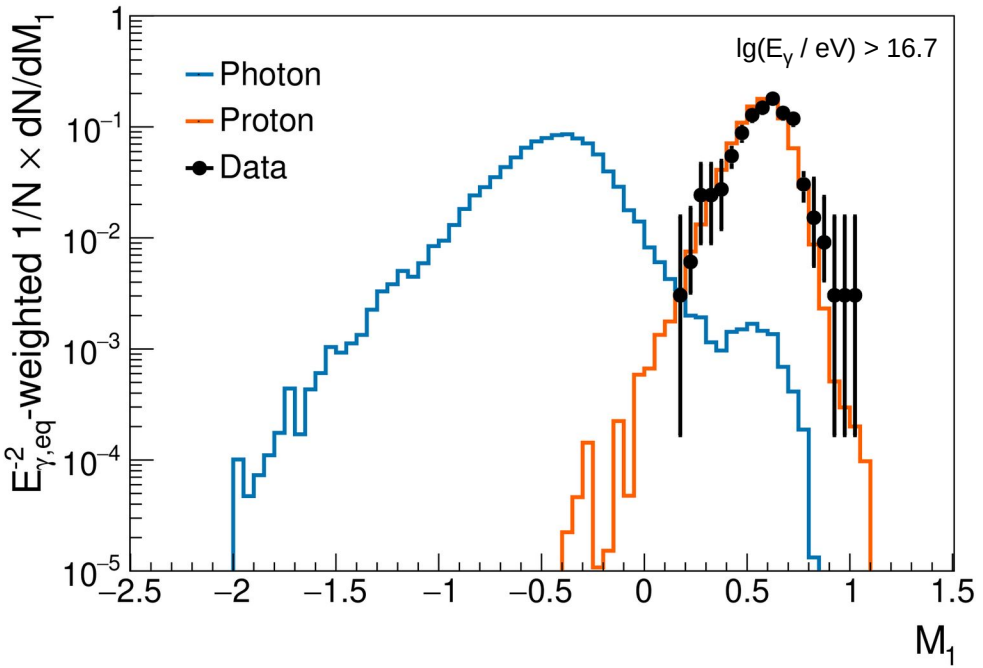

► 10% data from Cat I subset (329 events)

► Simulated events weighted as E^{-2}

► M_1 distribution for the burnt data is compatible with a hadronic origin

► Distribution for data artificially shifted towards lower values of M_1 (i.e., towards proton) due to energy scale:

- real events are assigned, on average, an energy 30% higher in the photon-equivalent scale
- these leads to a larger value of ρ_{pr} in M_1, thus to smaller values of M_1

$$M_1 = \lg\left(\sum_i \frac{\rho_i}{\rho_{\rm pr}} \times \left(\frac{r_i}{r_{\rm pr}}\right)\right)$$